Supporting information for

Mechanisms and plasticity of chemogenically-induced interneuronal suppression of principal cells

Stephanie Rogers[1#], Peter Rozman[1, 3#], Manuel Valero[1] Werner K. Doyle[3] and György Buzsáki[1, 2, 4, *]

[1]Neuroscience Institute, [2]Department of Neurology, [3]Department of Neurosurgery, Langone Medical Center, New York University, New York, NY 10016, USA
[4]Center for Neural Science, New York University, New York, NY 10003, USA

[#]These authors contributed equally

*Corresponding author: gyorgy.buzsaki@nyulangone.org

This file contains: Materials and Methods Figs. S1 to S8

SI Materials and Methods

Surgical Procedure. All experiments were approved by the Institutional Animal Care and Use Committee at New York University Langone Medical Center (NYULMC). Adult, male and female Sprague Dawley rats (200 – 350 g, 8 – 15 weeks of age) were used for viral injection and intracranial recordings. Rats were housed in pairs prior to implantation, but housed separately afterward and kept on a regular 12h – 12h light-dark cycle.

Virus Injection: Rats were initially anaesthetized with 2% isoflurane and maintained under anesthesia with 0.75 – 1% isoflurane during the surgery. Craniotomies were drilled bilaterally into the skull and the dura removed at each injection site. The coordinates targeted the dorsal and posterior parts of CA1. 1200 nL of pAAV-hDlx-GqDREADD-dTomato-Fishell-5 (a gift from Gordon Fishell; Addgene plasmid # 83896 ; http://n2t.net/addgene:83896 ; RRID:Addgene_83896) was infused into the hippocampus at a rate of 25 nL/minute using a sharp glass pipette (15 – 20 mm in diameter), which was left in place for 10 – 15 minutes following each injection to minimize the backflow of virus. The craniotomy site was covered with Kwik-Sil (World Precision Instruments) and the surgical opening was closed with sterile sutures. The animals were returned to their home cage for 1 – 2 weeks for recovery before the intracranial implantation was performed.

Intracranial implantation: The animals were initially anaesthetized with 2% isoflurane and maintained under anesthesia with 0.75 – 1% isoflurane during the surgery. The craniotomies were reopened and the dura removed for the implantation of silicon probes or tetrodes, which were mounted onto custom microdrives allowing for the precise movement of the probe following implantation, into the hippocampus (AP – 3.0, ML ± 1.6, DV – 1.8). Two stainless steel screws were drilled into the skull overlaying the cerebellum to serve as ground electrodes. The craniotomies were sealed and protected with a sterile silicon gel (Dow Corning Inc.). Rats recovered for 2-4 days before the recording probes were lowered gradually into the hippocampus. The exact depth of the recording sites was identified online by the characteristic layer-specific local field potential (LFP) patterns of the hippocampus (1).

Neurophysiological data acquisition. Neurophysiological recording sessions started at a fixed time each morning. During the first hour, baseline LFP and unit recordings were obtained while the animal was freely behaving or sleeping in its home cage. After an hour or occasionally longer, the animal received an intraperitoneal injection (either saline in 1% DMSO or 5 mg/kg CNO in 1% DMSO) and electrophysiological activity was recorded for the subsequent 4 – 12 hours with the rat freely behaving in its home cage. Three of the 51 recording sessions were excluded due to early disconnect (< 4 hrs) of the animal from the cable or other technical reasons.

LFP processing and state scoring. Hippocampal LFP was classified into wake (wake and RUN) and sleep state (nonREM and REM) epochs based upon LFP features, such as the theta/delta ratio calculated from the power spectrogram, electromyogram and movement information extracted from the synchronized onboard accelerometer (2).

Offline Detection of Sharp Wave-Ripple Complex. SPW-R complex detection followed a similar algorithm as previously described (3). For each session, two detector channels were manually identified: one for sharp-wave detection (str. radiatum) and one for ripple detection (str. pyramidale). First, the wide-band signal in both detector channels was band-pass filtered in the SPW frequency range (0.5-50 Hz, difference-of-Gaussians, *DOG*, zero-phase-lag, linear FIR) and the difference calculated between the two: the "SPW difference".

Next, the across-channel wide-band signal was subtracted from the wide-band signal in each detector channel and these signals were then band-pass filtered in the ripple frequency range (80-250 Hz, DOG, zero-lag, linear FIR). Instantaneous power was computed by rectifying and low-pass filtering, and identifying the across-channel maximum at each time point as the ripple power. The low-pass filter cutoff frequency corresponded to π cycles of the mean band-pass (52.6 Hz).

SPW-Rs were detected only during periods of immobility with low theta power. Three-point maxima in the sharp wave signal were identified in non-overlapping 250ms windows, with maximum ripple power in that window then logged. Only LFP events persisting longer than 20

ms with sharp waves not persisting longer than 500ms, and with sharp wave magnitude and ripple power exceeding 2.5 SD of the local background signal, were included in further SPW-R analysis.

For statistical analyses, sharp wave amplitude was calculated as the magnitude of the difference between a pyramidal layer site and a str. radiatum site, as described above. Note that because the amplitude of sharp wave varies as a function of the recording depth, amplitude comparisons are meaningful only within the same rat. Ripple amplitude was calculated as the amplitude of the ripple envelope at the time of ripple peak.

Histological processing. Rats were euthanized with sodium pentobarbital and transcardially perfused with 10% formalin. Whole brains were extracted and placed in 10% formalin overnight. 50 μm coronal sections were collected using a vibratome (Leica). Floating sections were incubated for 10 minutes at room temperature in blocking buffer (5% normal goat serum, 0.1% Triton X-100 in PBS) with DAPI. The sections were washed 3 times with PBS then mounted onto glass slides using Fluoromount-G (Sigma, USA). Confocal images of dTomato and DAPI were acquired using a Zeiss LSM510 and LSM800 confocal microscopes.

Spiking network simulations. We built a network model of leaky integrate-and-fire neurons using the Python-based simulator Brian2 (4). We included $n_{PYR} = 4000$ excitatory and $n_{INT} = 1000$ inhibitory neurons with the following random connection probability (c): $c_{PYR\text{-}PYR} = 0.05$, $c_{PYR\text{-}INT} = 0.1$, $c_{INT\text{-}INT} = 0.2$, $c_{INT\text{-}PYR} = 0.3$. The membrane potential of a neuron (i) obeys the following formula:

$$\tau_i \frac{dV_i}{dt} = -(V_i - E_L) + I_{rec}(t) + I_{ext,i}(t)$$

Where τ_i is the membrane time constant, E_L the leak potential, and $I_{rec}(t)$ and $I_{ext}(t)$ are the recurrent and external input terms, respectively. The following values were used for the τ and E_L constants: $\tau_{PYR} = 24$ ms, $\tau_{INT} = 10$ ms and $E_L^{PYR} = -55.8$ mV, $E_L^{INT} = -55.6$ mV. Whenever the membrane potential of the neuron i reaches the threshold V_{Th}, a spike is simulated, and the membrane potential was reset to V_{Res} with 1 ms of refractory period. The thresholds and resets values were $V_{Th}^{PYR} = -47$ mV, $V_{Th}^{INT} = -46.6$ mV and $V_{Res}^{PYR} = -52$ mV, $V_{Res}^{INT} = -51$ mV.

The recurrent input term consisted of the sum of all inhibitory and excitatory synaptic drives experienced by a given cell according to the rate of its presynaptic partners, and governed by:

$$\frac{dI_{rec}}{dt} = \frac{-g_{PYR,POST}}{\tau_E} - \frac{g_{INT,POST}}{\tau_I}$$

Where τ_X are the response time constants and $g_{PRE,POST}$ are the synaptic weights, with the following values for all combinations of synapses: $g_{PYR,PYR}$ = 1.76 mV, $g_{PYR,INT}$ = 1.0 mV, $g_{PYR,DSA}$ = 0.5 mV, $g_{INT,PYR}$ = – 0.8, $g_{INT,INT}$ = – 1, τ_E = 8.0 ms and τ_I = 2.0 ms.
The external input term includes a Gaussian white noise (ζi) term with σ = 4 mV and a time constant τ_{GWN} equal to the membrane time constant (τ_i). After the baseline period (10 s), E_L^{INT} was raised 1mV in 70% of all the interneurons, mimicking CNO activation. Code is available from: https://senselab.med.yale.edu/modeldb/.

Statistical Analyses. All analyses were performed in MATLAB 2019a software (Natick, MA). Continuous variables were compared using paired t-test for two-sample comparisons. For multiple comparisons, as in the case of multiple ripple features for each session, a conservative Bonferroni correction was applied. For comparisons of greater than two samples, a Kruskal-Wallis test with *post-hoc* multiple comparisons testing, or a Kolgomorov-Smirnov test was used for comparing cumulative distribution functions.

SI Figures and legends

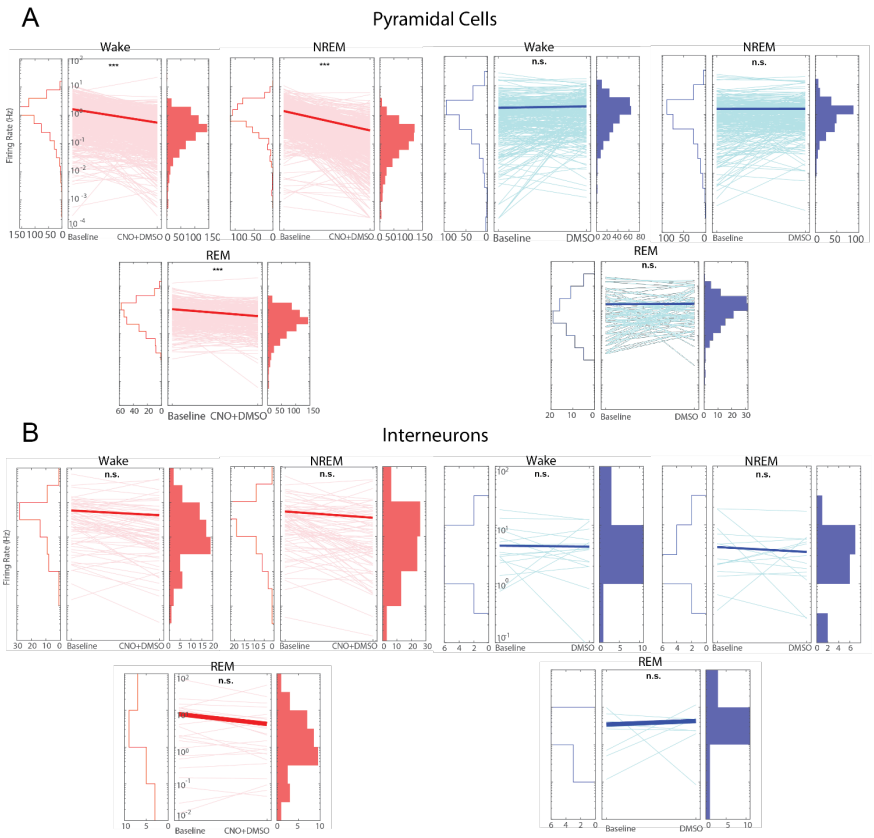

Fig. S1. The effect of CNO on firing rate is not dependent on brain state. Related to Fig. 2.
(A) Firing rate at baseline and after injection of CNO+DMSO *(red)* or DMSO only *(blue*) for pyramidal cells during wake (*panels 1 and 4*), nonREM sleep (*panels 2 and 5*), and REM sleep (*panels 3 and 6*). Firing rate changes significantly in both states for pyramidal cells in CNO+DMSO (*N* = 646, wake: p = 3.03×10^{-51}, nonREM: p = 1.05×10^{-75}, REM: 1.24×10^{-6}). It did not change significantly in DMSO only (*N=292,* wake: p=0.12, nonREM: p=0.62, REM: p=0.14). Up to one-hour-long epochs of each state at both baseline and after injection were included.
(B) Firing rate at baseline and after injection of CNO+DMSO *(red)* or DMSO only *(blue*) for interneurons during wake (*panels 1 and 4*), nonREM sleep (*panels 2 and 5*), and REM sleep (*panels 3 and 6*). Firing rate did not change significantly in any state after CNO+DMSO (*N=72,* wake: p=0.09, nonREM: p=0.09, REM: p=0.41) or DMSO only (*N = 19,* wake: p=0.86, nonREM: p=0.54, REM: p=0.78).
The number of cells included here is less than in Figure 1 due to state scores not being available for every recording. Concatenated epochs in each state of length up to one hour at baseline and after injection were included. Individual firing rates are shown in light blue and pink, average firing rate is shown in thicker red and blue lines. n.s. – not significant, *** - p<0.0001.

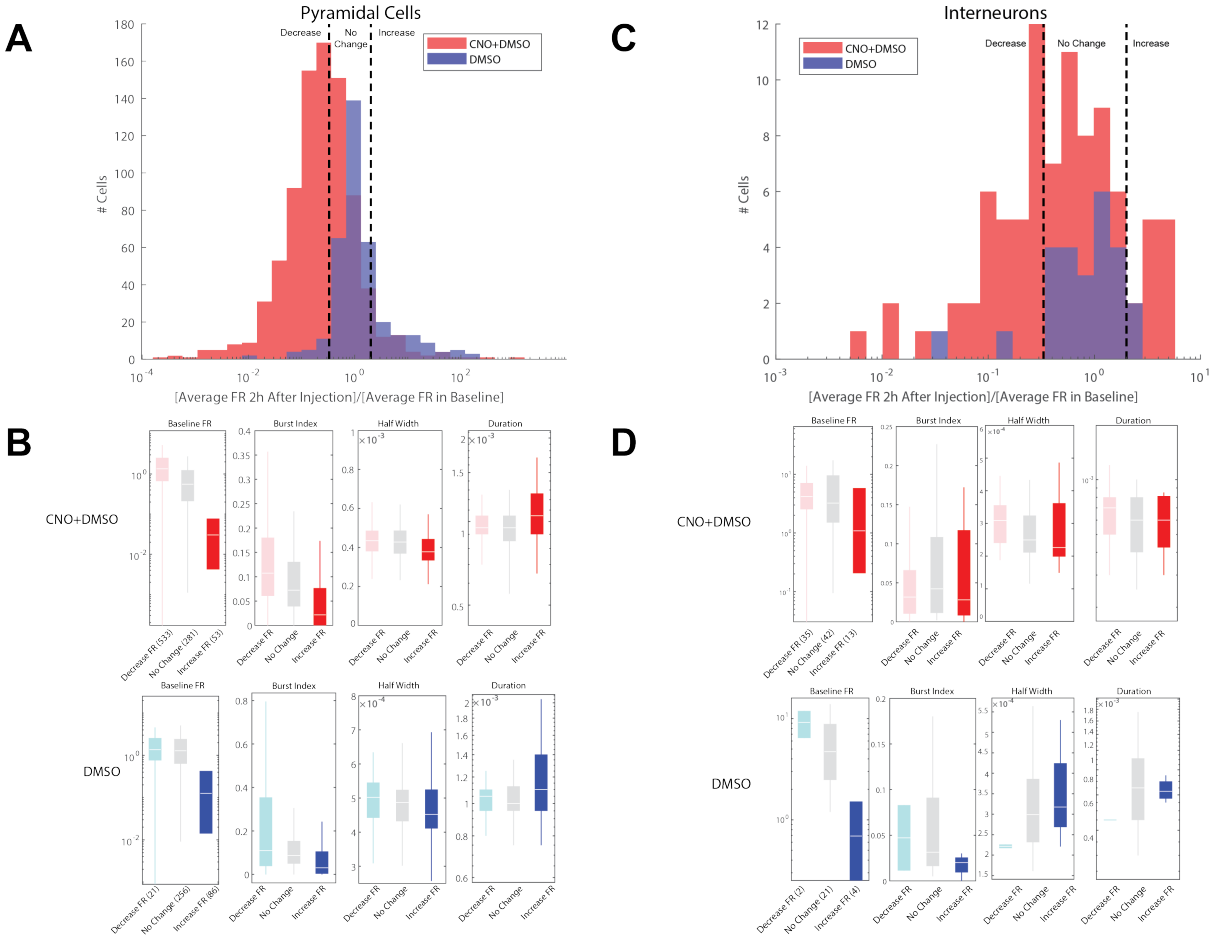

Fig. S2. Intrinsic cell properties are not associated with the response to CNO. Related to Fig. 2.
(A) Similar to **Figure 2D**, distribution of the ratio of pyramidal cell firing rates after injection of CNO+DMSO (*red*) or DMSO only (*blue*) versus at baseline. Cutoffs for decreased firing rate, no change in firing rate, and increased firing rate are indicated with dotted lines (at ratios of 0.33 and 2.0 for decreases and increases, respectively).
(B) Intrinsic pyramidal cell properties (burst index, baseline firing rate (Hz), half width (ms), and duration (ms)) for each category of change in response to injection of CNO+DMSO (*top, red*), and DMSO only (*bottom, blue*). Burst index is calculated as the fraction of interspike intervals (ISIs) < 6ms.
(C) and **(D).** Same layout as in (**A**) and (**B**) but for interneurons.

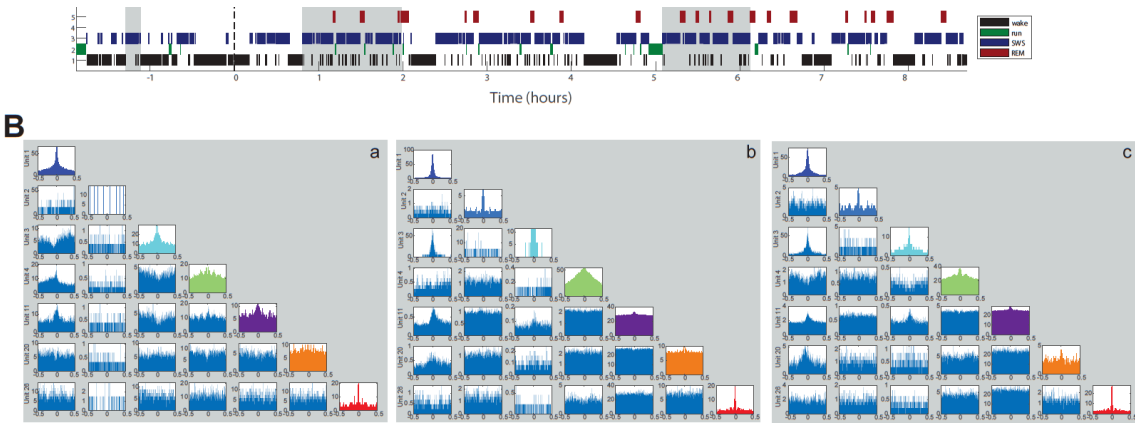

Fig. S3. Time-varied CA1 interneuron response to CNO injection, continued. Related to Fig. 3. **(A)** Same as panel A in Figure 3. *Top,* Z-scored firing rate (calculated in 60s window at 30s step) of all seven interneurons from a single session (rat #7, day #2). Unit numbers are indicated in the legend. *Bottom*, State scoring for this session with states indicated in legend. **(B)** Interneuron auto- and cross-correlograms from selected epochs. In this comparison, three largely nonREM (slow wave sleep; SWS) epochs were chosen (shaded in gray, labeled with lowercase letters). Epoch *a*, baseline, before injection of CNO+DMSO. Epoch *b*, approximately one-two hours after injection. Epoch *c*, five-six hours after injection. Note emergence of inversions (Unit 1-Unit 3 CCG, for example) and asymmetry (Unit 1-Unit 11 CCG, for example).

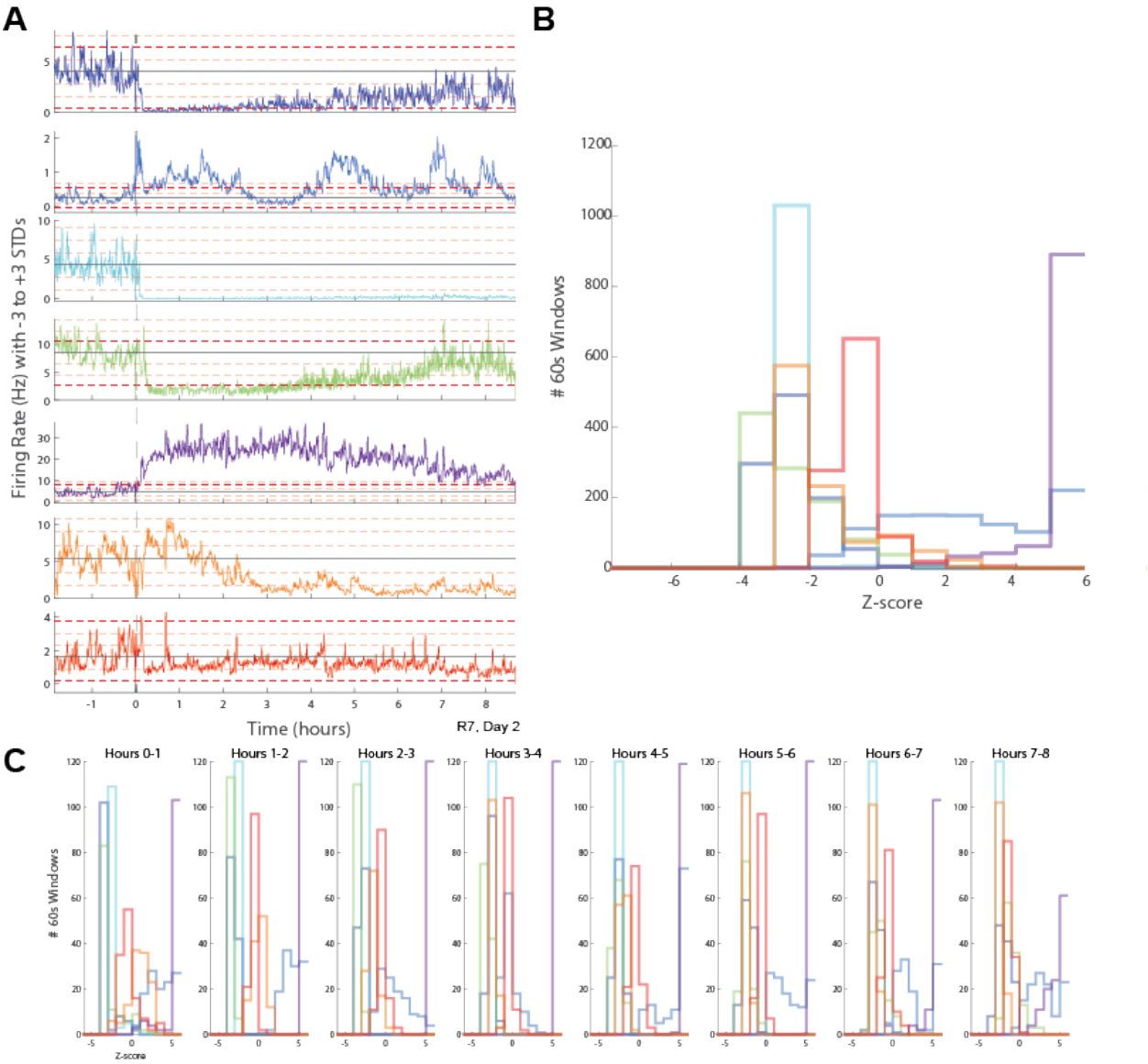

Fig. S4. Interneuron response to CNO injection over time. Related to Fig. 3.
(A) Absolute firing rate (Hz, calculated in sliding 60-second windows with 30-second step size) for each interneuron, colored as in Figure 3 and Supplemental Figure 3, for the same animal and session. ± 1, 2 and 3 SDs are also indicated (*dotted red lines*), as well as the baseline mean FR (*horizontal black line*).
(B) Distribution of Z-scores of each 60-second window for each interneuron (colored to match panel A) over the entire duration of the post-injection recording. Note that most interneurons either fire most often above or below the baseline mean firing rate.
(C) Distribution of Z-scores of each 60-second window for each interneuron as above, separated by hour post-injection. Cells tend to return to their baseline firing rate toward the end of this 8-hour session.

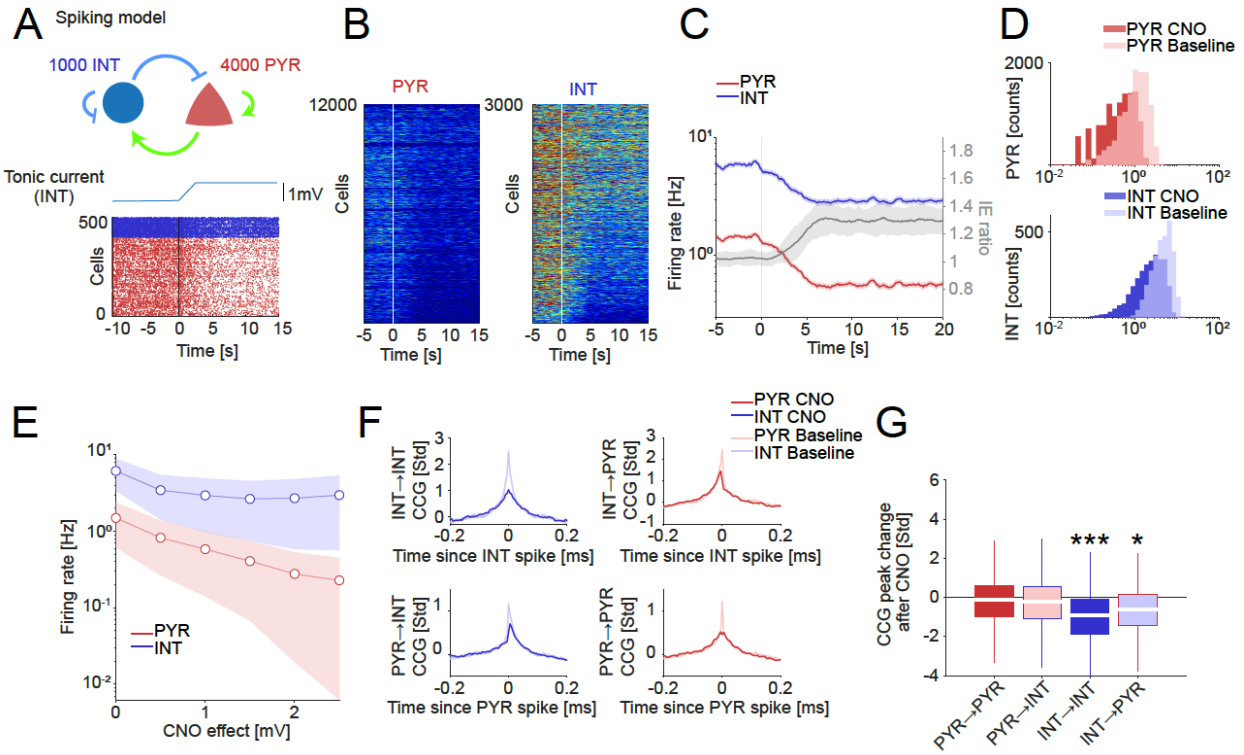

Fig. S5. Spiking neural network model of CNO/DREADDs effects. Related to Fig. 3.
(A) General structure of the model, containing 4000 pyramidal cells and 1000 interneurons (top). After the baseline period (10 s), a tonic depolarization was applied to the interneuron population, mimicking CNO activation. Spiking pattern distribution of population during the baseline period was tuned to match the experimentally obtained firing rate distributions (as in Fig. 2A). Not that both pyramidal cells and interneurons decreased that rates after mimicking uniform CNO activation of interneurons.
(B) Firing rate changes of pyramidal cells (left) and interneurons (right) after tonic depolarization. Each row shows a normalized color-coded rate of a single neuron.
(C) Simulated pyramidal cells (red) and interneuron (blue) firing rate changes as a function of time (mean ± IC95) after CNO simulation. Grey trace: Ratio of inhibitory (I) and excitatory (E) neuronal spikes in the same time windows. Note increased I/E ratio after CNO (interneuron depolarization)
(D) Group differences in distributions of firing rates for pyramidal cells (red) and interneurons (blue) during baseline and CNO simulation. Dark colors depict the baseline period (before CNO simulation), and light color shows neuronal firing rate after the tonic depolarization of the interneurons. Note decreasing firing rates of both pyramidal cells and interneurons.
(E) Pyramidal cells (red) and interneuron (blue) firing rate after the CNO simulation as a function of the increasing level of tonic excitation of the interneurons. Note that the E/I ration decreases monotonically as a function of the magnitude of tonic interneuron excitation.
(**F**) Z-scored cross-correlograms (CCG; mean ± IC95) for all cells grouped by class before and after the simulated CNO effect. All four combinations of neuron type pairs (INT→INT), (INT→PYR) (PYR→INT), (PYR-PYR) are shown. Note that (INT→PYR) and (PYR→INT) refer to the same data.
(G) Group difference (medians, interquartile ranges and error bars) of the Z-scored CCG changes after the tonic depolarization of the interneurons (simulated CNO effect) for all combination of simulated cell types. *P<0.05; ***P<0.001 from baseline.

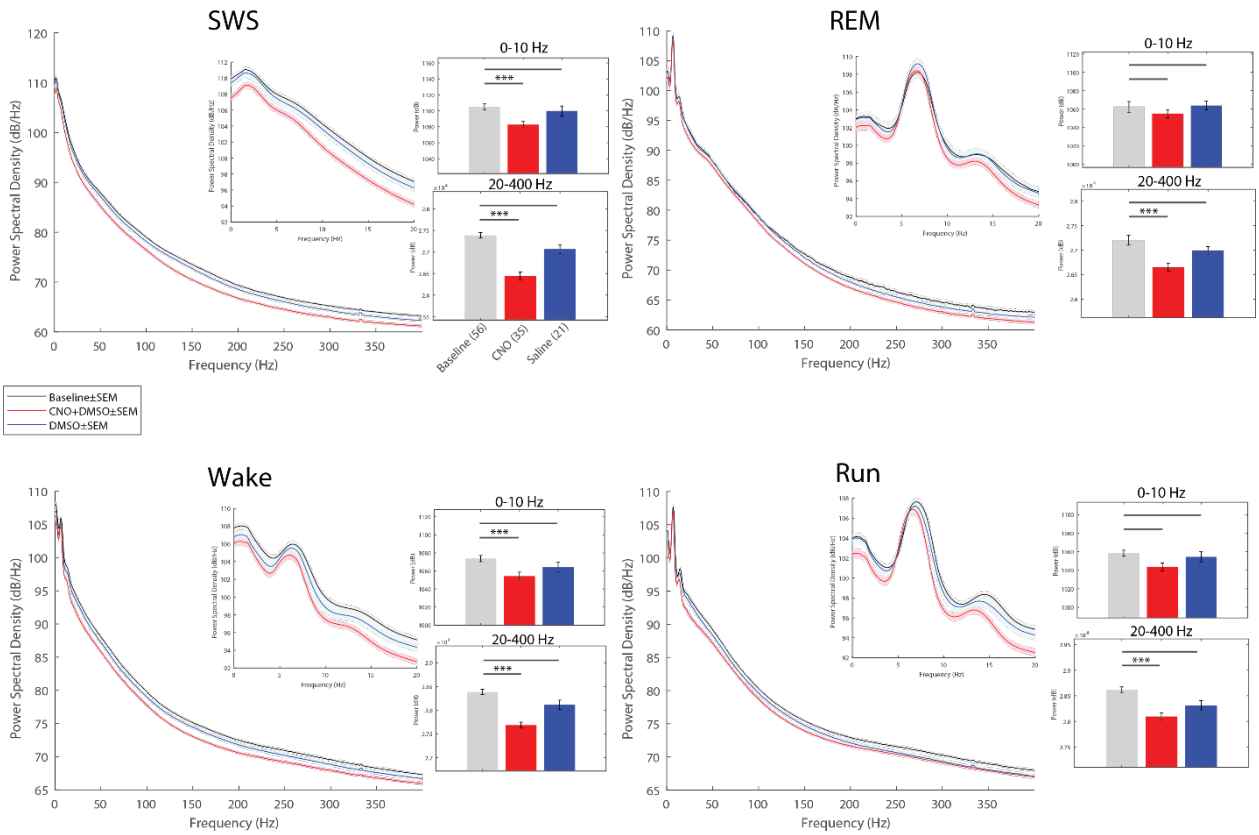

Fig. S6. LFP changes after CNO administration. Related to Fig. 6. Same layout as in Figure 6 but spectra were calculated from CA1 str. radiatum recordings.
Average state-specific power spectra over 0-400 Hz (large traces), and 0-20 Hz (insets) at baseline (*gray*) and after injection of CNO+DMSO (*red*) or DMSO only (*blue*). Sessions were state-scored to identify SWS, REM sleep, wake, and run states. Note the relative decrease in power spectral density after injection of CNO+DMSO in each state. Averaged band power for 0-10 Hz and 20-400 Hz is shown in the bar graphs for each state. Power after CNO injection was significantly affected for the 20-400 Hz band in each state and for the 0-10 Hz band in SWS and wake states. Power in the 0-10 Hz band was not significantly affected after CNO in REM sleep or while running, nor after DMSO injection in any state or frequency band. Differences were corrected for multiple comparisons using a Bonferroni correction. SWS – slow-wave sleep; REM – rapid eye movement. Note that power in the 0-20 Hz was significantly affected during nonREM and wake immobility but not during walking (Run) and REM.

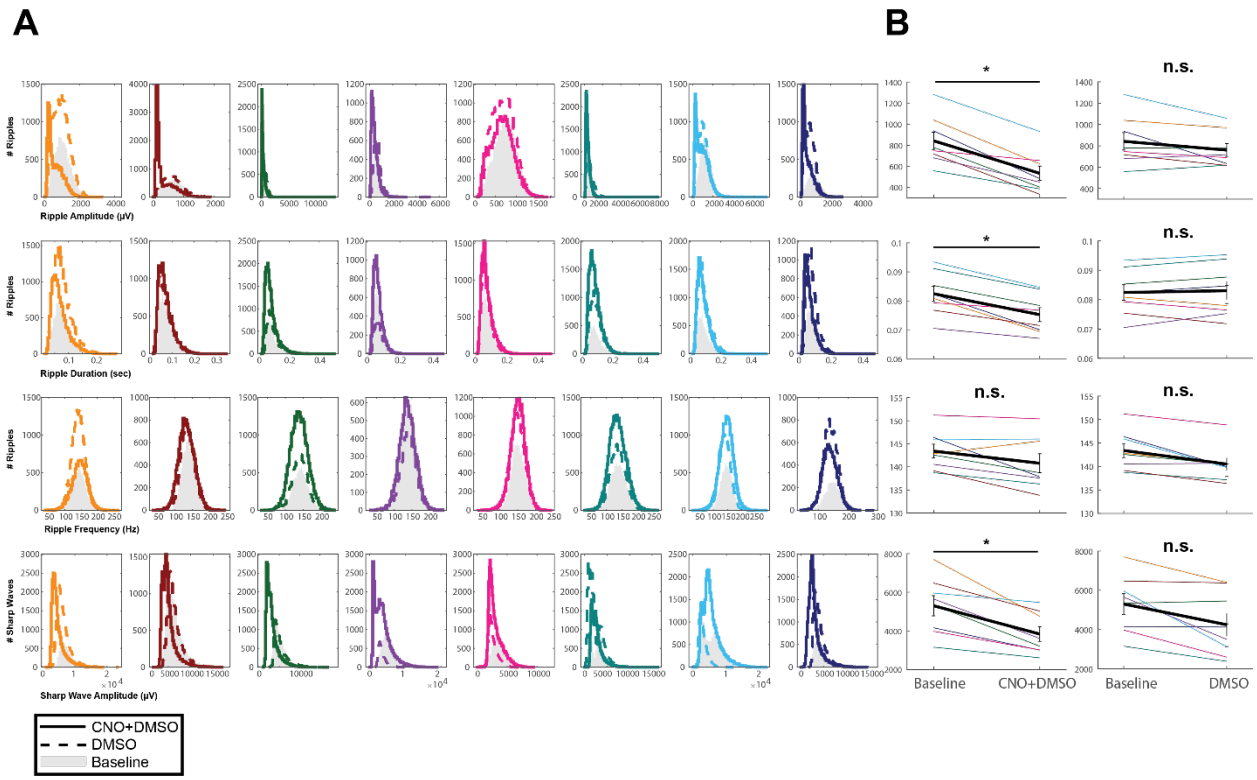

Fig. S7. Effect of CNO by SWR parameter and by subject. Related to Fig. 5.
(A) Distribution of SPW-R parameters (ripple amplitude, *row 1*, ripple duration, *row 2*, ripple frequency, *row 3*, sharp wave amplitude, *row 4*) for each rat (by column, as in Figure 5) at baseline (*gray filled histogram*), after injection of CNO+DMSO (*solid line*) and DMSO only (*dashed line*).
(B) Mean of each distribution (by color) in panel A, and overall mean±SEM (black line). * mark significant differences, after Bonferroni multiple comparisons correction. Values are show for baseline to injection of CNO+DMSO (left column) and baseline to injection of DMSO (right column).
Colors are assigned as in Figure 5, with each color representing the same rat as in Figure 5.

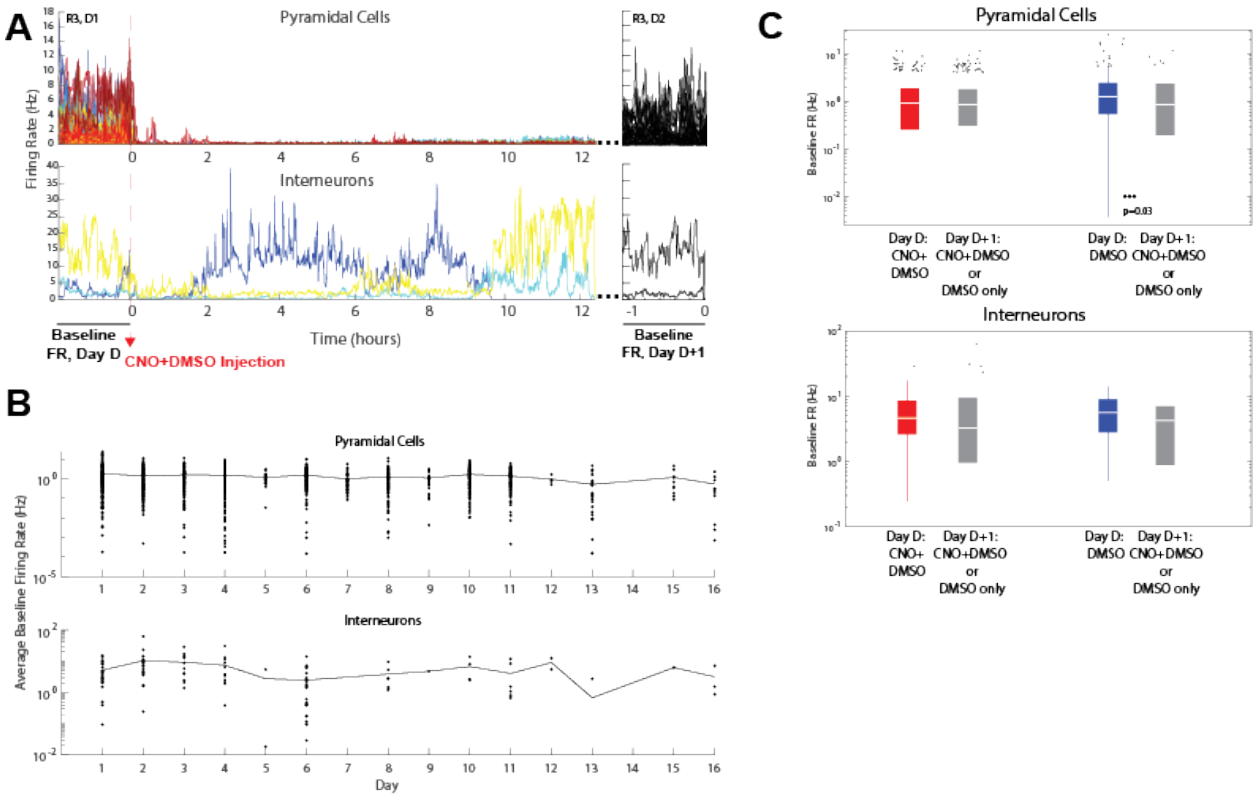

Fig. S8. Stability of baseline population firing rates. Related to Fig. 8.
(A) Representative session demonstrating longstanding effects of CNO injection on cell firing rate. Here, day 1 from rat 3, consisting of 39 pyramidal cells (*top*) and 3 interneurons (*bottom*), is shown with baseline recording, and post-CNO+DMSO recording indicated. Following this 12-hour session, the baseline from the following day, is shown. Not all units are the same from day to day. Of interest is whether this day 2 baseline recording differs from that of day 1.
(B) Baseline firing rates of every recorded unit sorted by experimental day. Pyramidal cells are plotted on top, with interneurons below. Black line connects the mean baseline firing rates at each day.
(C) Distribution of firing rates in (B), sorted into pairs of recording days, by whether the injection on the first day (day D) was CNO+DMSO (*red*) or DMSO only (*blue*). Injections on the second day (day D+1) could be either CNO+DMSO or DMSO only, as they have not yet occurred during the time of the baseline recording. Pyramidal cells before and after DMSO injection demonstrated a small difference in baseline firing rate (2.2 Hz on day D vs 1.5 Hz on day D+1, p=0.03). No other baseline rates significantly differed.

SI References:

1. A. Berényi, *et al.*, Large-scale, high-density (up to 512 channels) recording of local circuits in behaving animals. *J. Neurophysiol.* **111**, 1132–1149 (2014).
2. B. O. Watson, M. Ding, G. Buzsáki, Temporal coupling of field potentials and action potentials in the neocortex. *Eur. J. Neurosci.* **48**, 2482–2497 (2018).
3. E. Stark, *et al.*, Pyramidal cell-interneuron interactions underlie hippocampal ripple oscillations. *Neuron* **83**, 467–480 (2014).
4. M. Stimberg, R. Brette, D. F. Goodman, Brian 2, an intuitive and efficient neural simulator. *Elife* **8** (2019).